# Image Compression using Windowing Firefly Algorithm by Renyi 2-d Histogram based on Multilevel Thresholding

**V. Manohar[1†], G. Laxminarayana[2††], T. Satya Savithri[3†††]**

[1† 2†† 3†††] Department of Electronics & Communication Engineering, Jawaharlal Nehru Technological University, Hyderabad, 500 085, Telangana, India

**Summary**
Image compression is a significant process in image transmissions at high data rates over a communication channel. The main objective of the image compression is to extract meaningful clusters from a given image. A meaningful cluster is possible with perfect threshold values, which are optimized by assuming Renyi entropy as an objective function. Due to the equal distribution of energy over the entire 1-D histogram, it is computationally complex. In order to improve the visual quality of a reconstructed image, a 2-D histogram based multilevel thresholding is proposed to maximize the Renyi entropy using Windowing Firefly Algorithm (WFA). Thus procured results are compared with other optimization techniques and these are incorporated. It is the first time, incorporating a Weighted Peak Signal to Noise Ratio (WPSNR) and the Visual PSNR (VPSNR) in the proposed method, because of the failure in measuring the visual quality of Peak Signal to Noise Ratio (PSNR). Experimental results are examined on a standard set of images, which are observed precisely and efficiently in the multilevel thresholding problem.

***Key words:***
*Windowing Firefly Algorithm, Image Compression, 2-D histogram, thresholding, Renyi entropy.*

## 1. Introduction

Image compression is the process of encoding or converting an image file with less space than the original. It is a technique of reducing the number of bits, which are essential to enhance the storage capacity. Several methods were proposed for image compression in Joint Photographic Expert Group (JPEG) and JPEG-2000. Among these methods, few depend on mathematical transforms such as; Discrete Cosine Transforms (DCT) [1], Discrete Wavelet Transforms (DWT) [2], Integer Wavelet Transforms (IWT) [3], Karhunen Loeve Transforms (KLT) [4], Hartley Transform [5], Watershed Transform [6], Walsh Hadamard transform [7], Tchebichef Transform [8] and Singular Value Decomposition (SVD) [9].
Various clustering algorithms [10] were developed for image compression and derived into two main classifications: Hierarchical and Partitional algorithms. The hierarchical algorithm finds successive clusters using earlier established clusters and it can be agglomerative (bottom-up) or divisive (top-down), whereas Partitional algorithm determines all clusters at a time. Non-transformed methods are also used in image compression like Vector Quantization and Thresholding. Extracting background image is a challenging task in selecting a gray level threshold from image processing. Thresholding techniques are upholding various real-time applications in progressive robustness, accuracy and less time convergence. There are two ways to approach thresholding, parametric and non- parametric. The main disadvantage of a parametric approach is excessive time consumption, while in non parametric approach, as in Otsu's method it is carried on class variance which depends upon the conditions of entropies.
Based on the intensity values, the fundamental assumption of thresholding methods is to classify the object and background. These can be classified into bi-level and multi-level thresholding. In bi-level, only one threshold is opted to divide the image into two classes, whereas in multi-level, more than one threshold must be determined. Detailed research on image thresholding is classified into six categories [11], based on Clustering, Entropy, Histogram shape, Object attribute, spatial and local methods. Considering histograms of the gray level images, Kapur classified the images based on calculating threshold [12]. The image is divided by evaluating the variance of pixel intensities according to the Otsu's method [13]. The moment preserving principle [14] is for effective and efficient color image thresholding. Kaur et al [15] follows a particular approach to select the wavelet packets with low computational cost which optimizes the operational rate-distortion (R-D), thresholds and quantizers in order to develop JTQ-WP. Wavelet domain thresholding depends on Partial Differential Equation (PDE) for noise removal and image compression. Image compression is developed to minimize the quantization error in Multistage Lattice vector quantization (MLVQ) [16]. An inbuilt mat lab function was used by Siraj [17] for the compression i.e. Birge–Massart thresholding and the outcomes are compared to unimodal thresholding. Its drawback is the exponential rise of CPU time and to overcome this problem, evolutionary and swarm-based calculation techniques are opted. Particle Swarm Optimization (PSO) is developed for usual image compression [18] based on 2-D DWT image thresholding with the support of swarm

Manuscript received March 5, 2019
Manuscript revised March 20, 2019

evolutionary and optimization method. In case of excessive particle velocity, the PSO undergoes uncertainty and requires more tuning parameters [19].

In this paper, a novel algorithm is presented to improve the quality of threshold selection by exploiting the statistical properties of input image. In the proposed method (WFA), we select initial threshold centers based on image density in each area of Euclidean space. For this, distribution function of the training thresholds magnitude is estimated by Parzen windowing method. Since the proposed algorithm uses the statistical properties instead of probabilistic search, it is faster than the compared evolutionary optimization algorithms. The proposed algorithm is applied for effective thresholding with the help of 2-D histogram and assumed Renyi entropy as a fitness function which is optimized. The obtained results are compared with 1-D histogram and other optimization techniques. The compressed image is further compressed with encoding techniques like run-length and arithmetic coding. The objective value, PSNR, WPSNR, and VPSNR are taken into consideration for improvement of 2-D histogram-based image thresholding when compared to other algorithms.

## 2. Concept of Renyi Entropy

Let's assume an *'n'* array finite discrete probability distributions such as $(F_1, F_2, F_3 \ldots F_n) \varepsilon \Delta_n$ where $\Delta_n = \{(F_1, F_2, F_3 \ldots F_n), F_i \geq 0, i = 1, 2, 3....n, n \geq 2, \sum_{i=1}^{n} F_i = 1\}$ with random variables $(X_1, X_2, X_3, \ldots\ldots X_n)$ then Renyi entropy for independent and additive random events as per Eq.(1).

$$H_\alpha = \frac{1}{1-\alpha}\log_2\left(\sum_i^n F_i^\alpha\right) \quad (1)$$

Where *'α'* is greater than zero, it is known as entropy order. When *'α'* tends to one, then Renyi entropy becomes Shannon entropy. In general, the image is the combination of two clusters; one carries object information *(Cluster C1)* (Eq. 2) and the another carries background *(Cluster C2)* (Eq. 3) then Renyi entropy is

$$H_\alpha[C_1] = \frac{1}{1-\alpha}\left[\log_2\left(\sum_{i=0}^{t}\left(\frac{F(\mathrm{i})}{F(C_1)}\right)^\alpha\right)\right] \quad (2)$$

$$H_\alpha[C_2] = \frac{1}{1-\alpha}\left[\log_2\left(\sum_{i=t+1}^{L-1}\left(\frac{F(\mathrm{i})}{F(C_2)}\right)^\alpha\right)\right] \quad (3)$$

Where $\mathrm{F}(C_1) = \sum_{i=0}^{t} F(\mathrm{i})$ , $\mathrm{F}(C_2) = \sum_{i=t+1}^{L-1} F(\mathrm{i})$ Here $F_i$ is the normalized one dimensional histogram of the image and *'L'* is highest intensity level of gray scale image. The overall renyi entropy for a given image with one threshold *'t'* is given as

$$\varphi_\alpha(t) = argmax(\left[H_\alpha[C_1] + H_\alpha[C_2]\right]) \quad (4)$$

### 2.1 Multi-Level Thresholding

Let image is divided into *'N'* number of clusters $C = (C_1, C_2, C_3 \ldots C_N)$ with *N* number of threshold values $t = (t_1, t_2, t_3 \ldots t_N)$ then Renyi entropy for each individual cluster is defined in Eq.(5),(6) and (7) [20]

$$H_\alpha[C_1] = \frac{1}{1-\alpha}\left[\log_2\left(\sum_{i=0}^{t_1}\left(\frac{F(\mathrm{i})}{F(C_1)}\right)^\alpha\right)\right] \quad (5)$$

$$H_\alpha[C_2] = \frac{1}{1-\alpha}\left[\log_2\left(\sum_{i=t_1+1}^{t_2}\left(\frac{F(\mathrm{i})}{F(C_2)}\right)^\alpha\right)\right] \quad (6)$$

$$H_\alpha[C_N] = \frac{1}{1-\alpha}\left[\log_2\left(\sum_{i=t_N-1}^{L-1}\left(\frac{F(\mathrm{i})}{F(C_N)}\right)^\alpha\right)\right] \quad (7)$$

Here, $\mathrm{F}(C_1) = \sum_{i=0}^{t_1} F(\mathrm{i})$ , $\mathrm{F}(C_2) = \sum_{i=t_1+1}^{t_2} F(\mathrm{i})$ , $\mathrm{F}(C_N) = \sum_{i=t_N-1}^{L-1} F(\mathrm{i})$ the overall Renyi entropy or objection function for a given image for N thresholds as per Eq.(8).

$$\varphi_\alpha(t) = argmax(\left[H_\alpha[C_1] + H_\alpha[C_2] + \ldots H_\alpha[C_N]\right]) \quad (8)$$

For simplifying the calculations, two dummy thresholds are introduced $t_0$ and $t_N = L\text{-}1$ which satisfies the condition $t_0 < t_1 \ldots < t_{N-1} < t_N$. The optimal thresholds are obtained by maximizing the above equation with any soft computing techniques.

### 2.2 Two-Dimensional Renyi Entropy:

Let *I (m,n)* is an image intensity at spatial location *(m,n)*. In digital image *[I (m, n)| m ε {1, 2, 3..., M}, n ε {1, 2, 3..., N}]*, where *M, N* are size of the image and its 1-D histogram *h(x)* for *x ε {1, 2, 3…, L-1}*, where *'L'* is *256* for gray scale image. Let us denote elements in histogram *{1, 2, 3… 255}* as *G*. In literature, optimal thresholds selections are based on 1-D histogram and are obtained by optimizing the objective function/entropy. The 2-D histogram of an image is obtained by defining a local average of pixel, *I(x,y)*, as the average intensity of its nine neighbors denoted as *g(x,y)* as per Eq.(9) [21].

$$G(x,y)=\frac{1}{9}\sum_{i=-1}^{1}\sum_{j=-1}^{1}f\left(x+i,y+j\right) \quad (9)$$

For example, let us take an image of size $4\times4$ as shown in Fig 1 (a) and its average intensity *g(x,y)* is calculated by padding required number of zeros at edges as shown in Fig. 1(b).The First table in Fig.1(a) is an image and first element i.e. 126, *g(x,y)* is calculated by padding zero's at edges and the last table in Fig.1(c) shows *g(x,y)* for entire image *I(x,y)*. In Fig. 2 the .2-D histogram of Lena image of marked area is represented, where diagonal quadrants carry much information.

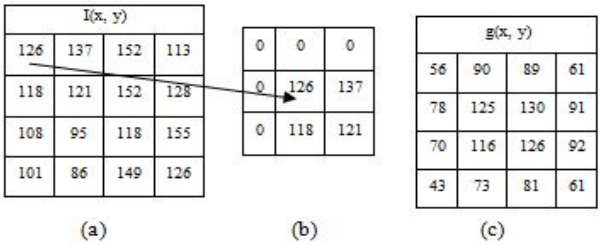


Fig. 1 Example for 2-D histogram calculation

The 2-D histogram of tested images as shown in Fig. 2 are classified into four clusters by a single threshold *(t,s)*. Where *t* is threshold for original image intensity *I(x,y)* and *s* is threshold for average intensity image *g(x,y)*. The divided cluster area is not same. The 1st diagonal quadrant represents object, 3rd represent background whereas 2nd and 4th quadrants are neglected because they do not carry any information (pair occurrence is less) as show in Fig. 2. The Renyi entropy for Object and background is given as per Eq.(10) and (11).

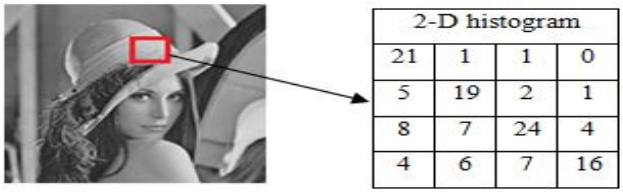


Fig. 2 Lena image and 2-D histogram

$$H_{object}^{\alpha}[t,s]=\frac{1}{1-\alpha}\left[\log_2\sum_{i=0}^{t}\left(\sum_{j=0}^{s}\left(\frac{F(i,j)}{F_{D1}(t,s)}\right)^{\alpha}\right)\right] \quad (10)$$

$$H_{background}^{\alpha}[t,s]=\frac{1}{1-\alpha}\left[\log_2\sum_{i=t+1}^{L-1}\left(\sum_{j=s+1}^{L-1}\left(\frac{F(i,j)}{F_{D2}(t,s)}\right)^{\alpha}\right)\right] \quad (11)$$

Where

$$F_{D1}(t,s)=1-\sum_{i=0}^{t}\sum_{j=0}^{s}F(i,j) \quad \text{and} \quad F_{D2}(t,s)=1-\sum_{i=t+1}^{L-1}\sum_{j=s+1}^{L-1}F(i,j)$$

The final objective function which is to be maximized for better threshold (t, s) selection is shown in Eq. (12).

$$\varphi_{\alpha}(t)=argmax\left(\left[H_{object}^{\alpha}[t,s]+H_{background}^{\alpha}[t,s]\right]\right) \quad (12)$$

## 2.3 Proposed Renyi 2d-Hisotgram Based Multi-Level Thresholding

The 1-D histogram delivered inferior results in multilevel thresholding due to incorrect selection of thresholds. For which, a 2-D histogram is developed with superior results in multilevel thresholding. It has gained lots of popularity in dividing the image into several useful clusters for accurate examination and understanding the image. We proposed a Renyi 2-D histogram for image compression based on multilevel thresholding. The 2-D histogram of an image is separated into 9 clusters with two thresholds ($t_1$, $t_2$) and ($s_1$, $s_2$) as shown in Fig.3 (a). Then the diagonal quadrants 1st, 5th, and 9th represent objects(s) Eq.(13), intermediate regions Eq.(14) and background Eq.(15) respectively as illustrated in Fig.3(a) and ignored the rest of the regions like noise and edges. The Renyi entropy of diagonal quadrants is given as

$$H_{object}^{\alpha}[t,s]=\frac{1}{1-\alpha}\left[\log_2\sum_{i=0}^{t_1}\left(\sum_{j=0}^{s_1}\left(\frac{F(i,j)}{F_{D1}(t,s)}\right)^{\alpha}\right)\right] \quad (13)$$

$$H_{intermediate}^{\alpha}[t,s]=\frac{1}{1-\alpha}\left[\log_2\sum_{t_1+1}^{t_2}\left(\sum_{s_1+1}^{s_2}\left(\frac{F(i,j)}{F_{D2}(t,s)}\right)^{\alpha}\right)\right] \quad (14)$$

$$H_{backgroud}^{\alpha}[t,s]=\frac{1}{1-\alpha}\left[\log_2\sum_{t_2+1}^{L-1}\left(\sum_{s_2+1}^{L-1}\left(\frac{F(i,j)}{F_{D3}(t,s)}\right)^{\alpha}\right)\right] \quad (15)$$

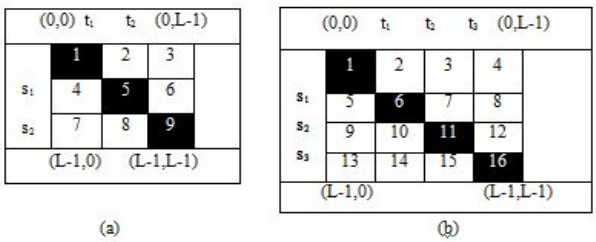


Fig. 3 2-D histogram for a) 3- level b) 4- level

Where

$$F_{D1}(t,s) = 1 - \sum_{i=0}^{t_1}\sum_{j=0}^{s_1} F(i,j) \quad , \quad F_{D2}(t,s) = 1 - \sum_{i=t_{1+1}}^{t_2}\sum_{j=s_1+1}^{s_2} F(i,j)$$

and $F_{D3}(t,s) = 1 - \sum_{i=t_{2+1}}^{L-1}\sum_{j=s_2+1}^{L-1} F(i,j)$.

The final objective function which is to be maximized for better threshold (t, s) selection as per Eq.(16)

$$\varphi_\alpha(t) = argmax([H^\alpha_{object}[t,s] + H^\alpha_{intermediate}[t,s] + H^\alpha_{background}[t,s]]) \quad (16)$$

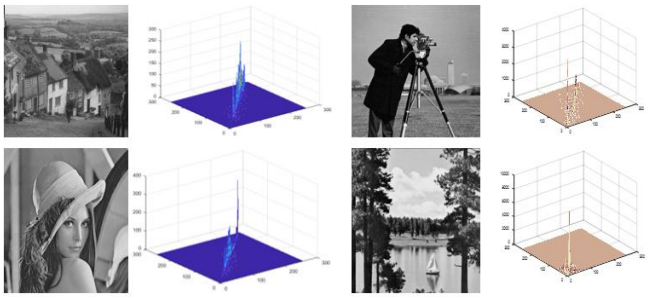

Fig. 4 Input images and corresponding 2-D histogram

The Eq.(16) can be extended for 'N' threshold values as shown as per Eq.(17).

$$\varphi_\alpha(t) = argmax([H_1^\alpha[t,s] + H_2^\alpha[t,s] + H_3^\alpha[t,s].. .....H_{N+1}^\alpha[t,s]) \quad (17)$$

Where

$$H_k^\alpha[t,s] = \frac{1}{1-\alpha}[\log_2 \sum_{i=t_{k-1}+1}^{t_k}(\sum_{j=s_{k-1}+1}^{s_k}(\frac{F(i,j)}{F_{Dk}(t,s)})^\alpha)] \quad (18)$$

For simplifying the calculations, two dummy thresholds are introduced $t_0$ and $t_{N+1} = L-1$ which satisfy the condition $t_0 < t_1 \ldots < t_{N-1} < t_{N+1}$. Similarly two dummy variable $s_0$ and $s_{N+1} = L-1$ which satisfy the condition $s_0 < s_1 < s_{N-1} < s_{N+1}$.The 2-D histogram of four standard images is shown in Fig.4. It is observed that most of the information/energy is concentrated on diagonal quadrants. Multilevel thresholding is a time-consuming process and is proportional to the number of thresholds 'N'. So, soft computing techniques play a significant role in this contest by assuming Eq. (17) as an objective function, which leads to a reduction in the computational time.

## 3. Overview of Firefly Algorithm

### 3.1 Firefly Algorithm

The performance of Honey Bee Mate optimization (HBMO) technique depends on various inter-reliant parameters needed to be tuned for efficient codebook design, which is a difficult task for the researchers [22]. So the Firefly algorithm (FA) was developed by Xin She Yang in 2009 [23]. It is based on the flashing pattern and behavior of fireflies which basically depends on the phenomenon of bioluminescence. Here, Fireflies are inspired by the flashing pattern and characteristics of fireflies. The underlying advantage of flashing lights is that a brighter firefly will attract other less brighter fireflies and this phenomenon consequently allows fireflies to explore the search space, i.e., update their positions. The brightness (fitness) of every firefly is calculated using the objective function [24].

The FA algorithm detailed is given below.

Step 1: Select the fireflies/ thresholds randomly and its corresponding tuning parameters, population size, maximum iteration.

Step 2: Initialize $\alpha$, $\beta$ and $\gamma$ parameters and rest of the thresholds with random numbers.

Step 3: Find out fitness values of each population by Eq. (17).

Step 4: Randomly select a population and record its fitness values. If the population is with higher fitness value, then it moves towards the brighter codebook (highest fitness value) based on the Eq. (19) - (21).

Euclidean distance ($r_{ij}$) is

$$r_{ij} = \left\| x_i - x_j \right\| = \sqrt{\sum_{k=1}^{N_c}\sum_{h=1}^{L}(x_{i,k}^h - x_{j,k}^h)^2} \quad (19)$$

Here, $x_i$ is randomly selected codebook, $x_j$ is brighter codebook.

$$\beta = \beta_0 e^{-\gamma_{i,j}} \quad (20)$$

$$x_{j,k}^h = (1-\beta)x_{i,k}^h + \beta x_{j,k}^h + u_{j,k}^h \quad (21)$$

Where $\mu_{j,k}$ is random number between 0 to 1, k=1,2,…..,$N_c$, h=1,2,….L.

Step 5: If selected firefly doesn't find brighter fireflies in search space, then it moves randomly as per Eq.(22).

$$x_{i,k}^h = x_{i,k}^h + u_{j,k}^h \qquad k=1, 2... N_c, \quad h=1, 2,….L \quad (22)$$

Step 6: Repeat steps (3) to (5) until one of the termination criteria is reached.

In ordinary firefly algorithm at step 5, when no such brighter fireflies are found in search space, then fireflies move randomly which leads to local optimal solution. So, in this paper the randomness is eliminated by Parzen–Rosenblatt window method. This modification in firefly is called windowing firefly algorithm.

### 3.2 Parzen–Rosenblatt window method

Parzen-Rosenblatt window method is a nonparametric method to estimate the probability density function of a random variable [25] which also known as Kernel Density Estimation. In comparison, parametric estimators have a constant functional structure and the elements of this function are the only information needed to store. In Nonparametric estimators have no constant structure and depend upon all the data points to achieve an estimate.
Let $x$ be a random variable with an unknown density function $f(x)$. Parzen-windowing estimates the $p(df)$ of random variable samples $(x_1, x_2, \dots, x_n)$. The kernel density estimator for $x$ is calculated as per Eq. (23).

$$f_h(x) = \frac{1}{N}\sum_{i=1}^{N} K_h(x - x_i) = \frac{1}{Nh}\sum_{i=1}^{N} \mathrm{K}\left(\frac{x - x_i}{h}\right) \quad (23)$$

Where $K(.)$ is the Kernel function, $h>0$ is a smoothing parameter (the bandwidth), kernel with subscript $h$ (scaled kernel). A range of kernel functions such as uniform, triangular, normal, and others are commonly used. Due to its convenient mathematical properties, the normal (Gaussian) kernel is often used as per Eq. (24).

$$\mathrm{k(x)} - \mathrm{G(x)} = \frac{1}{\sqrt{2\Pi}} e^{\frac{-x^2}{2}} \quad (24)$$

The bandwidth $h$ controls the degree of smoothing and strongly influences the resulting estimate.

### 3.3 Proposed Windowing Firefly Algorithm (WFA)

The ordinary firefly algorithm may follow into local optimal when no such brighter fireflies in the search as discussed in the *step 5* of firefly algorithm, So windowing firefly algorithm is proposed which avoids the uncertainty in the algorithm. This technique follows a specific strategy in selecting the initial thresholds. In this method, K-dimensional image space is segmented into non-overlapping areas and then according to data density in each of these areas, the initial threshold centers are chosen. In order to segment the space into non-overlapping areas, Euclidean norm measure is used. The Euclidean norm of a threshold, in k-dimensional image space, is calculated as per Eq.(25):

$$\| x \| = \sqrt{\sum_{i=0}^{k} x_i^2} \quad (25)$$

The position of a point in Euclidean $k$-dimensional space is a Euclidean distance. Now, consider Fig.5 that shows a data set of training threshold in 2-dimensional space. This Fig.5 displays width and length of the petals from Fisher's Iris data set as per this data set as set I.

Fig. 5(a) shows estimated probability density function of Euclidean lengths for training vectors of set I. By integration of the probability density function of Euclidean lengths f(r) on different areas, an estimation of data density in each area is achieved. The number of initial cluster centers (thresholds) in each region must be proportional to the density of data in that region.

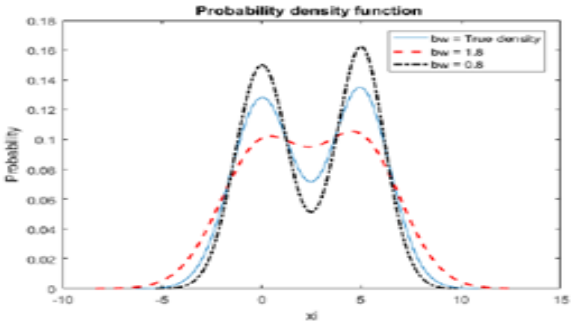


Fig. 5(a). Kernel density estimate (KDE) with different bandwidths

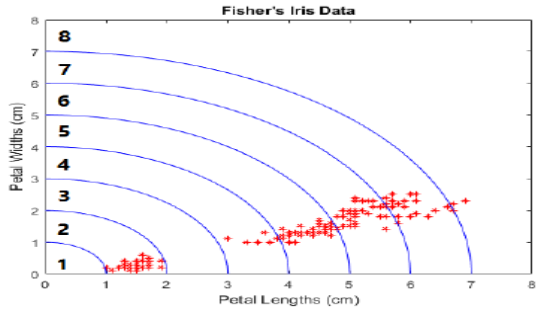


Fig. 5(b) Investigation of data density in different areas of 2-dimensional space for training vectors of set I.

Table 1: Shows data density in each area for training vectors in set I.

| Region | Euclidean norm(cm) | Data density |
|---|---|---|
| 1 | R<1 | 0% |
| 2 | 1<R<2 | 32% |
| 3 | 2<R<3 | 0% |
| 4 | 3<R<4 | 5% |
| 5 | 4<R<5 | 22% |
| 6 | 5<R<6 | 23% |
| 7 | 6<R<7 | 14% |
| 8 | 7<R | 4% |

As per Fig. 5 (b), space areas are divided into 8 segments based on their magnitudes. As it is seen that data density is not uniformly distributed in different segments, random selection of the initial threshold centers is not the best possible choice. To have a better choice, initial threshold centers should be selected according to data density in each area. In order to obtain data distribution in different areas, distribution function of the training thresholds should be estimated using Parzen windowing method with a kernel function.

### 3.4 Performance of proposed algorithm on benchmark functions

Prior to the proposal of any new optimization algorithm, its performance should be tested on some common and well known functions called benchmark functions. In this paper, six benchmark functions namely Ackely, Alpine, Exponential, Griewank 1 and 2, Powell Singular are selected for testing the proposed algorithm shown in Fig.6. From the above said functions, the performance of the proposed algorithm (WFA) is tested on Differential evaluation (DE), Particle swarm optimization (PSO) and ordinary firefly algorithm (FA). From Fig. 6, it is observed that the performance of WFA is better than other algorithms such as DE, PSO and FA. All functions are optimized in which WFA gives a less value.

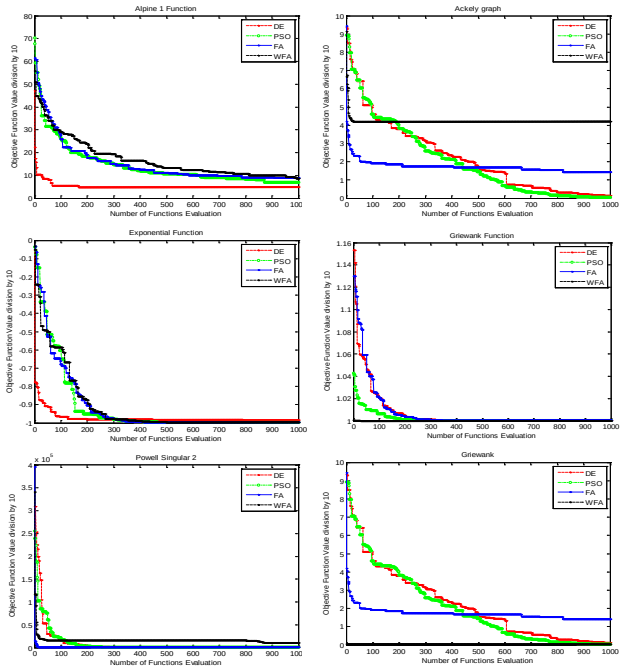


Fig. 6 Benchmark functions of Ackely, Alpine, Exponential, Griewank 1 and 2, Powell Singular

The proposed WFA flowchart is shown in Fig. 7.

## 4. Results and Discussion

The proposed algorithm is evaluated by considering the standard benchmark images like Lena, Gold hill, Lake, and Cameraman with all the images of size *256×256* and each pixel takes *8* bits (bits per pixel = 8). The images of Cameraman and Leena are in '.tif' format except for Lake (.gif) and Gold hill (.jpeg) format. All the algorithms are simulated in Mat lab version 2017 and implemented in desktop with specifications: Windows 7 Enterprise N, HP Compaq LE1902x, Intel (R) Core (TM) Duo CPU e7500N at 2.93GHz, 64-bit operating system. The number of iterations (itr) = 50, population size *P = 100*, upper bound *Ub = 255*, *Lb = 0*, dimensions of the problem *D = th*, which are considered for all optimization algorithms. In this paper, number of thresholds *th = 5* is opted for all algorithms. The performance of WFA is examined by thresholding the image using 1-D, 2-D histogram and differentiated with the outcomes of DE, PSO, and BA for same tuning parameters.

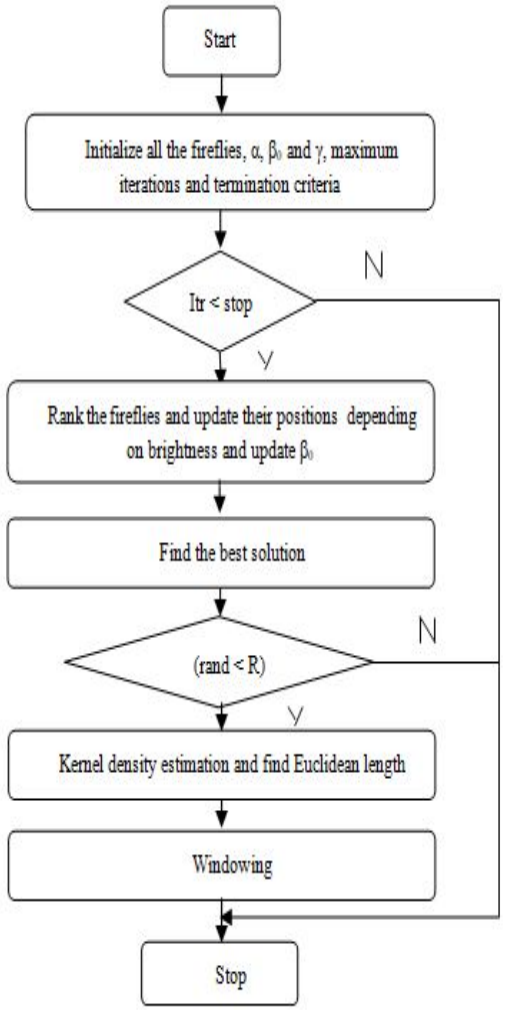


Fig. 7 Flowchart of proposed Windowing Firefly Algorithm (WFA)

### 4.1 Quantitative validation

To maximize the objective function and Standard Deviation, all the algorithms are optimized. Table 2 displays the objective function for WFA, BA, DE, and PSO. Hence, from Table 2 by using Renyi entropy, the objective value obtained with 2-D histogram for different

images is higher than 1-D histogram. The proposed WFA objective value is greater than other algorithms with both histograms.

Table 2: Comparison of Objective value and Standard deviation for various algorithms

| | | Objective value | | Standard deviation | |
|---|---|---|---|---|---|
| Images | Opt. Tech | 1-D histo gram | 2-D histo gram | 1-D histo gram | 2-D histo gram |
| Camera Man | DE | 18.5687 | 21.2727 | 0.0012 | 0.1245 |
| | PSO | 18.5965 | 21.2311 | 0.1478 | 0.0147 |
| | BA | 18.6145 | 21.3589 | 0.3587 | 0.1479 |
| | WFA | 18.8112 | 21.5123 | 0.0944 | 0.2698 |
| Lena | DE | 18.2578 | 21.1245 | 0.1012 | 0.1478 |
| | PSO | 18.3589 | 21.3785 | 0.1208 | 0.2587 |
| | BA | 18.4589 | 21.3738 | 0.2454 | 0.6587 |
| | WFA | 18.5998 | 21.5014 | 0.9876 | 0.5643 |
| Gold Hill | DE | 18.2354 | 21.0124 | 0.2478 | 0.0147 |
| | PSO | 18.2945 | 21.1245 | 0.9875 | 0.0195 |
| | BA | 18.3012 | 21.2458 | 0.2578 | 0.0782 |
| | WFA | 18.5432 | 21.5688 | 0.3119 | 0.7865 |
| Lake | DE | 18.9012 | 21.1245 | 0.3698 | 0.2547 |
| | PSO | 18.9147 | 21.2354 | 0.2478 | 0.3214 |
| | BA | 18.4587 | 21.5478 | 0.2475 | 0.1245 |
| | WFA | 18.9298 | 21.7654 | 0.1123 | 0.0098 |

## 4.2 Mean Square Error (MSE) and Peak Signal to Noise Ratio (PSNR)

The PSNR illustrate variations between the threshold image and original image. In general, it reconstructs better quality for the indication of higher value. As per Eq. (26) to calculate Peak signal to noise ratio shown below.

$$PSNR = 10 \times \log_{10}\left(\frac{(255^2)}{MSE}\right) \quad (26)$$

As per Eq. (27) to calculate Mean square Error (MSE) value, $Y$ is output image and $X$ is input image, $M \times N$ is size of the image shown below.

$$MSE = \frac{1}{M \times N}\Sigma_{i=1}^{M}\Sigma_{j=1}^{N}(x_{ij} - y_{ij})^2 \quad (27)$$

The values which are attained for PSNR from the different algorithms are shown in Table 3 and this proposed algorithm attained better PSNR values with the 2-D histogram. So, the quality of the reconstructed images gets much improved for the higher level thresholds. It is observed that 2-D histogram achieves higher PSNR values compared to 1-D and quality of reconstructed image is improved along with decrement of MSE as in Table 3.

Table 3: Comparison of PSNR & MSE values for different algorithm

| | | PSNR | | MSE | |
|---|---|---|---|---|---|
| Images | Opt. Tech | 1-D histo gram | 2-D histo gram | 1-D histo gram | 2-D histo gram |
| Camera Man | DE | 26.1258 | 28.5689 | 158.672 | 90.4045 |
| | PSO | 26.3589 | 28.6358 | 150.380 | 89.0226 |
| | BA | 26.3587 | 28.8987 | 150.387 | 83.7935 |
| | WFA | 26.4956 | 29.0688 | 136.295 | 76.4537 |
| Lena | DE | 26.1478 | 29.0147 | 157.870 | 81.5850 |
| | PSO | 26.2587 | 29.2587 | 153.89 | 77.1277 |
| | BA | 26.3687 | 29.2958 | 150.041 | 76.4716 |
| | WFA | 26.6543 | 29.6198 | 113.979 | 69.1779 |
| Gold Hill | DE | 26.6589 | 28.2587 | 140.342 | 97.0980 |
| | PSO | 26.6698 | 28.3658 | 139.991 | 94.732 |
| | BA | 26.8578 | 28.4789 | 134.060 | 92.2975 |
| | WFA | 26.9999 | 28.8797 | 112.767 | 75.3182 |
| Lake | DE | 26.8915 | 28.8698 | 133.024 | 84.3529 |
| | PSO | 26.9991 | 28.9879 | 129.768 | 82.0900 |
| | BA | 27.0145 | 29.0147 | 129.309 | 81.5850 |
| | WFA | 27.2241 | 29.2005 | 111.037 | 61.7701 |

## 4.3 Weighted PSNR (WPSNR)

The WPSNR is precise and [26] incorporate the human visual system into account while measuring the resemblance between the input and processed images. The WPSNR in dB as per Eq.(28).

$$WPSNR = 10 \times \log_{10}\left(\frac{(255)^2}{NVF \times MSE}\right) \quad (28)$$

NVF = Noise Visibility Function expressed as

$$NVF = norm\left(\frac{1}{1+\delta_{block}^2}\right) \quad (29)$$

Where, δ block is standard deviation for f blocks of pixels, it is close to zero in smooth regions and close to unity in edges/textures. From Table 4 it is observed that projected technique WPSNR is improved with the 2-D histogram compared to 1-D.

## 4.4 Visual-PSNR (VPSNR)

Sometimes PSNR doesn't match with image expert mean opinion scores (MOS). So that visual PSNR [27] is measured by considering visual MSE and contrast masking aspect of the human visual system (HVS). VPSNR outperforms existing SSIM, FSIM, and WPSNR. The visual MSE is calculated by partitioning the input and output image into n blocks, X and Y are input and reconstructed images respectively, N is image size and K is size of the partitioned image block then visual MSE is given as per Eq.(30).

$$VMSE_K = \frac{MSE_K}{1 + 0.5\sqrt{\sigma_X^K + \sigma_Y^K}} \quad K=1, 2, 3.....N \qquad (30)$$

Where $MSE_K = \frac{1}{n}\sum_{i=1}^{n}(X_i^k - Y_i^k)^2$ and standard deviation of the block is evaluated as follows

$\sigma_X^K = \sqrt{\frac{1}{n-1}}\sum_{i=1}^{n}(X_i^k - U_i^k)^2$ and $U_i^K = \frac{1}{n}\sum_{i=1}^{n} X_i^k$

Then VPSNR is given as in Eq. (31)

$$VPSNR = 10 \times \log_{10}\left(\frac{(255^2)}{\overline{MSE}}\right) \qquad (31)$$

Where, $\overline{MSE} = \frac{1}{N}\Sigma_{k=1}^{N} MSE_K$

Table 4 illustrates the projected technique VPSNR, which is improved with the 2-D histogram.

Table 4: WPSNR & VPSNR values for different algorithms

| | | WPSNR | | VPSNR | |
|---|---|---|---|---|---|
| Images | Opt. Tech | 1-D histo gram | 2-D histo gram | 1-D histo gram | 2-D histo gram |
| Camera Man | DE | 14.258 | 13.568 | 15.568 | 15.256 |
| | PSO | 14.721 | 15.578 | 16.258 | 16.124 |
| | BA | 16.257 | 15.124 | 17.478 | 17.102 |
| | WFA | 18.889 | 19.342 | 19.999 | 19.354 |
| Lena | DE | 14.981 | 15.987 | 14.457 | 16.909 |
| | PSO | 14.879 | 17.578 | 14.698 | 18.024 |
| | BA | 15.124 | 17.157 | 16.457 | 18.245 |
| | WFA | 17.321 | 18.546 | 20.085 | 19.888 |
| Gold Hill | DE | 14.143 | 19.999 | 14.102 | 18.214 |
| | PSO | 15.698 | 20.247 | 16.247 | 19.247 |
| | BA | 15.999 | 21.127 | 16.367 | 22.124 |
| | WFA | 17.909 | 22.003 | 18.454 | 22.354 |
| Lake | DE | 15.457 | 15.147 | 16.957 | 18.608 |
| | PSO | 15.951 | 16.258 | 17.547 | 18.425 |
| | BA | 16.124 | 17.369 | 18.654 | 19.962 |
| | WFA | 17.432 | 19.342 | 19.344 | 20.766 |

## 4.5 Qualitative Results

The processed images and histogram attained with proposed 2-D histogram, which is based on WFA algorithm at threshold level 5 with Renyi entropy is shown in Fig. 7. At a upper level of threshold *(th = 5)* it is noticed that visual quality of constructed image is much better than *th=2, 3* and *4*. Lena image at *th=5* as in Fig. 7a and Cameraman at *th=5* as in Fig. 7b is observed that WFA visual quality is better with 2-D histogram compared to 1-D. Similarly, Gold hill image at *th=5* as shown in Fig.7c and Lake Image at *th=5* as shown in Fig.7d are relatively good and improved when compared to the earlier algorithms with reference to visual quality. In Fig. 7d, the background is not visible in the Lake image with 1-D histogram, whereas it is clearly visible with a 2-D histogram.

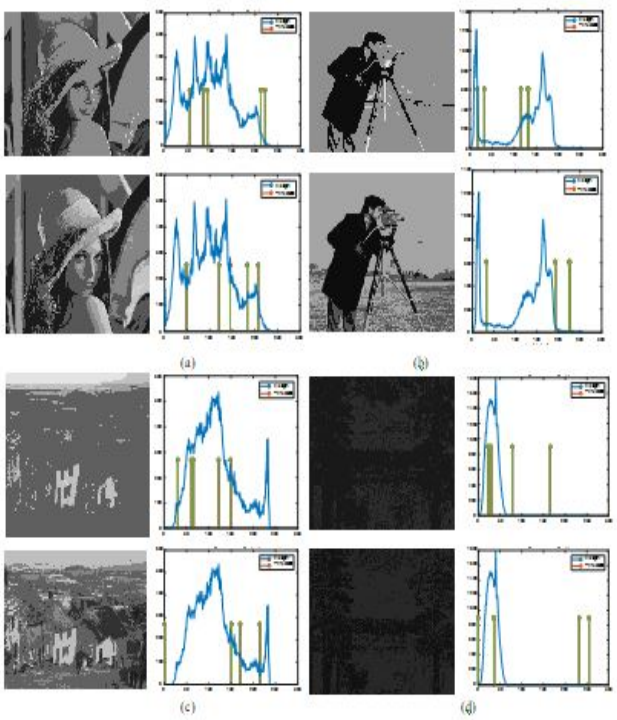

Fig. 7 Reconstructed images and subsequent optimal thresholds a) Lena b) Cameraman c) Gold hill d)Lake

## 5. Conclusions

In this paper, Windowing Firefly Algorithm (WFA) with 2-D histogram is based on multi-level image thresholding for compression of image by maximizing the Renyi entropy for effective image thresholding. WFA is successfully tested on standard test images to illustrate the performance of algorithm. The procured outcomes of the WFA are compared to algorithms such as DE, PSO, and BA with Renyi entropy. With these comparisons, it is viewed that the projected algorithm (WFA) has a maximum fitness value among other algorithms. The projected algorithm has concluded the high PSNR, VPSNR, and WPSNR values for the improved eminence of projected technique.

## References


[1] R. T. Haweel, W. S. El-Kilani and H. H. Ramadan, "Fast approximate DCT with GPU implementation for image compression", Journal of Visual Communication and Image Representation, vol. 40, Part A, pp. 357 - 365, 2016.

[2] T.Bruylants, A.Munteanu and P.Schelkens, "Wavelet based volumetric medical image compression", Signal Processing: Image Communication, vol.31, pp.112-133, 2015.

[3] M. Zhang and X. Tong, "Joint image encryption and compression scheme based on IWT and SPIHT", Optics and Lasers in Engineering, Vol. 90, pp. 254 - 274, 2017.

[4] G. M. Zhang, T. Olofsson and T. Stepinski, "Ultrasonic NDE image compression by transform and sub band coding", NDT &E International,vol.37,pp.325-333,2004.

[5] R.S. Sunder, C. Eswaran, and N. Sriraam, "Medical image compression using 3-D Hartley transform", Computers in Biology and Medicine,vol.36,pp.958-973,2006.

[6] W. Y. Hsu, "Improved watershed transform for tumour segmentation: Application to mammogram image compression", Expert Systems with Applications, vol. 39, pp. 3950 - 3955, 2012. doi:10.1016/j.eswa.2011.08.148

[7] D.Venugopal, S.Mohan and S. Raja,"An efficient block based lossless compression of medical images", Optik, vol. 127, pp. 754 - 758, 2016. doi:10.1016/j.ijleo.2015.10.154

[8] M. Kiruba and V. Sumathy, "RPF-DTT: Register Pre-allocation based Folded Discrete Tchebichef Transform (DTT) Architecture for Image compression", Integration, the VLSI Journal, vol. 60, pp.13 - 24, 2018.

[9] M. Kumar and A. Vaish, "An efficient encryption-then compression technique for encrypted images using SVD", Digital Signal Processing, vol. 60, 99. 81 - 89, 2017.

[10] X. Han, L. Quan, X. Xiong, M. Almeter, J. Xiang, and Y. Lan, "A novel data clustering algorithm based on modified gravitational search algorithm ," Engineering Applications of Artificial Intelligence, vol. 61, pp. 1-7,2017.

[11] Sezgin. M, B. Sankur, "Survey over image thresholding techniques and quantitative performance evaluation", Electronics and Imaging, vol. 13, pp. 146-165, 2004.

[12] J. N. Kapur, P. K. Sahoo, and A. K. C. Wong, A new method for gray-level picture thresholding using the entropy of the histogram, Computer Vision Graphics Image Processing vol. 29, pp. 273-285,1985. doi: 10.1016/0734-189X (85)90125-2

[13] Otsu. N, "A threshold selection from gray level histograms" IEEE Transa on System, Man and Cybernetics, vol. 66, 1979.

[14] Yang Chen kuei, Wen.H "Color image compression using quantization thresholding and edge detection techniques all based on the moment preserving principle". Patterns recog letters, vol.19, pp.205-215, 1998.

[15] Kaur L, Gupta S, Chauhan R C, Saxena S C, "Medical ultrasound image compression using joint optimization of thresholding quantization and best-basis selection of wavelet packets." Digital Sig Processing, vol.17, pp.189–198, 2007.

[16] Salleh. M. F. M and Soraghan. J, "A New Multistage Lattice Vector Quantization with Adaptive Sub-band Thresholding for Image Compression", EURASIP Journal on Advances in Signal Processing Dec, 2007. doi:10.1155/2007/92928

[17] Siraj. S, "Comparative study of Birge–Massart strategy and unimodal thresholding for image compression using wavelet transform" Optik, vol.126, pp. 5952-5955, 2015.

[18] Sallari Kaveh Ahmadi, Ahmad Y. Javaid, Ezzatollah Salari, "An efficient compression scheme based on adaptive thresholding in wavelet domain using particle swarm optimization" Signal Processing: Image Communication, vol. 32, pp. 33–39, 2015.doi:10.1016/j.image.2015.01.001

[19] Rini. D. P, Shamsuddin.S. M and Yuhaniz. S. S, "Particle Swarm Optimization: Technique, System and Challenges", International Journal of Computer Applications (0975 - 8887) vol. 14, No.1, 2011

[20] Rényi, A, "On measures of information and entropy", In Proceedings of the 4th Berkeley symposium on mathematics, statistics and probability, pp.547–561, 1960.
[21] Soham S and Swagatam Das, "Multilevel Image Thresholding Based on 2D Histogram and Maximum Tsallis Entropy A Differential Evolution Approach", IEEE Transactions On Image Processing, vol. 22, No. 12, pp. 4788, 2013. doi:10.1109/tip.2013.2277832
[22] Afarandeh.E , Yaghoobi .M, Bolouri M, "Fractal image compression by local search and honey bee mating optimization", 5th International Conference on Computer Sciences and Convergence Information Technology, Seoul, South Korea,2010.
[23] Yang, X.-S, "Firefly algorithms for multimodal optimization". In International symposium on stochastic algorithms. Springer, pp.169–178, 2009.
[24] Chandra Sekhar. G.T, Sahu. R. K, Baliarsingh. A. K, and Panda. S, "Load frequency control of power system under deregulated environment using optimal firefly algorithm", Elect Power and Energy Systems, vol.74 pp. 195–211, 2016.
[25] Man Hua**,** Yanling Li ,Yinhui Luo, "Robust Background Modeling with Kernel Density Estimation, Online Engineering Innovations based on Intelligent Information Processing, vol.11 issue 8, pp 13-15 ,2015.
[26] Navas. K. A, Gayathri Devi K. G, Athulya M. S, Anjali Vasudev, "MWPSNR: A new image fidelity metric", IEEE Recent Advances in Intelligent Computational Systems (RAICS), pp. 627-632, 2011.
[27] Alexander. T, "Visual-PSNR measure of image quality", Journal of Visual Commun. and Image Repre, vol. 25, pp. 874-878, 2014. doi:10.1016/j.jvcir.2014.01.008

**V.Manohar** received his Bachelor's degree in 2005 and Master's engineering degree in 2010 in Electronics and Communication Engineering from Jawaharlal Nehru Technological University, Hyderabad, India. At present he is pursuing Ph.D Degree in Electronics and Communication Engineering in JNT University, Hyderabad, India. He is a member of IETE & ISTE. His research areas are Image Processing, Optimization Techniques and Wireless Communications.

**Dr.G.Laxminarayana** received his Bachelor's degree in Electronics and Communication Engineering from Osmania University, Hyderabad, India and Master's engineering degree from Indian Institute of Science, Bangalore, India and Ph.D from Jawaharlal Nehru Technology University, Hyderabad, India in Department of Electronics and Communication Engineering. He is a member of IETE & IEEE and ISOI. His research areas are VLSI, Wireless Communications and GPS.

Dr. T. Satya Savithri, is presently working as Professor in ECE Department of JNTUH Colleg of Engineering, Hyderabad, India. Her research interests include, Digital Image Processing, Design and Testing of VLSI and also Wireless communications. She has 125 publications in various national and International Journals and Conferences. She has 22 years of teaching experience. She has obtained her B. Tech degree from NIT Warangal, M.E from Osmania and PhD in Digital Image Processing from JNTU Hyderabad. Presently, she is guiding 8 students at Ph.D. level.